mathematics

MDPI

Article

On the Dynamics of Fractional Models for Power Systems with Incommensurate Orders: Chaos, Multistability, and Control

Omar Kahouli [1,*], Nadjette Debbouche [2], Adel Ouannas [3], Sulaiman Almohaimeed [4], Lilia El Amraoui [5] and Mohamed Ayari [6,*]

1 Department of Electronics Engineering, Applied College, University of Ha'il, Ha'il 2440, Saudi Arabia
2 Department of Sciences, Teacher Education College of Setif, P.O. Box 556, Setif 19600, Algeria
3 Department of Mathematics, Faculty of Science, Islamic University of Madinah, Madinah 42351, Saudi Arabia
4 Department of Electrical Engineering, College of Engineering, Qassim University, Qassim 52571, Saudi Arabia; sulaiman.m@qu.edu.sa
5 Department of Electrical Engineering, College of Engineering, Princess Nourah Bint Abdulrahman University, P.O. Box 84428, Riyadh 11671, Saudi Arabia
6 Department of Information Technology, Faculty of Computing and Information Technology, Northern Border University, Arar 91431, Saudi Arabia
* Correspondence: omarkahouli@yahoo.fr (O.K.); mohamed.ayari@nbu.edu.sa (M.A.)

Abstract

This paper presents the nonlinear chaotic dynamics of a power system model within an incommensurate fractional-order framework. Equilibrium points are derived and analyzed using Jacobian-based local stability theory adapted to fractional-order systems. Furthermore, bifurcation analysis is employed to examine how variations in system parameters and incommensurate fractional orders influence the emergence of period-doubling cascades and chaotic motion. The study investigates multistability phenomena characterized by the coexistence of multiple attractors under identical system parameters. The simulation is run in MATLAB R2020a, and nonlinear tools such as time series, bifurcation diagrams, Lyapunov exponents, and phase portraits in 2D and 3D projections are used to visualize the findings.

Keywords: power system; incommensurate fractional-order; multistability; coexisting attractors; bifurcation; chaos

MSC: 34C28

1. Introduction

Power systems are inherently nonlinear dynamical systems whose behavior is strongly influenced by generator dynamics, network topology, and load characteristics [1,2]. Small variations in system parameters or operating conditions may significantly affect system stability, leading to complex nonlinear phenomena such as equilibrium bifurcations, oscillatory responses, and chaotic motion. In particular, the loss of stability of equilibrium points through period-doubling bifurcations represents one of the most important routes to chaos in power system dynamics, potentially resulting in voltage instability and degraded system performance.

Chaos in power systems is characterized by strong sensitivity to initial conditions and parameter variations, which complicates both analysis and control. Classical integer-order models have been widely used to investigate such behaviors; however, these models often neglect memory and hereditary effects that naturally exist in physical components such as

Academic Editors: Roman Ivanovich Parovik and Zhouchao Wei

Received: 14 April 2026
Revised: 6 August 2026
Accepted: 12 August 2026
Published: 2 September 2026

 https://doi.org/10.3390/math14173164

generators, transmission lines, and loads. As a result, integer-order modeling may fail to fully capture the true dynamic characteristics of real-world power systems [3–6].

Fractional-order derivatives offer a robust and adaptable mathematical framework for modeling systems characterized by memory effects and long-term dependence. By extending the notion of differentiation to non-integer orders, fractional-order models introduce extra degrees of freedom that have a big effect on how systems behave. Recent studies have demonstrated that the fractional derivative order itself can act as a critical system parameter, affecting equilibrium stability, shifting bifurcation points, and altering the onset and structure of chaotic behavior [7].

Recent advances in fractional-order power-system research have further demonstrated the effectiveness of fractional calculus in modeling complex dynamical phenomena and enhancing system performance. In particular, secure control strategies for incommensurate fractional-order cyber-physical power systems have been developed to improve resilience against communication attacks [8]. Fractional-order techniques have also been successfully employed for load-frequency regulation in interconnected power networks with energy-storage units [9]. Furthermore, model-free fractional-order excitation stabilizers have shown promising results in enhancing transient stability in multi-machine power systems [10]. More recently, fractional discrete-time power-system models have revealed rich dynamical behaviors, including chaos, complexity, and control-related phenomena, highlighting the growing importance of fractional-order approaches in modern power-system analysis [11].

The interplay of chaos and fractional-order dynamics produces complicated and distinct phenomena that do not exist in standard integer-order systems. The stability of equilibrium points in fractional-order systems is influenced by both the eigenvalues of the Jacobian matrix and the fractional order of the derivative. As a result, stability zones vary, and the transition from stable equilibrium to periodic motion and chaos often through period-doubling bifurcations can occur under quite different conditions than in integer-order models [12].

Chang was recently the subject of a study in [13] that examined the dynamics of a power system with three machines, with a particular emphasis on chaos control and complex nonlinear dynamics. The research uncovered a diverse array of dynamics across a range of parameter values in the bifurcation diagram. Additionally, ref. [14] established a continuous feedback control method that is predicated on synchronization characteristics to mitigate erratic oscillations. An additional investigation conducted by P.C. Gupta and P.P. Singh regarding the modeling and nonlinear analysis of a multi-machine system utilizing swing dynamics is examined in [15], which uncovers the existence of coexisting attractors (multistability). The same authors conducted a nonlinear study and management of a fractional-order small-scale grid (SSG) in [16], investigating disturbances and noise, including multistability and the coexistence of multiple attractors, together with a period-doubling route to chaos. In [17], a thorough investigation was performed on the dynamic behavior of a fractional-order three-machine infinite bus (TMIB) power system model employing Grunwald-Letnikov's technique. It is essential to acknowledge that prior research exclusively examined comparable fractional-order derivatives. The examination of incommensurate fractional-order nonlinear systems is critically important, as it provides a more accurate and flexible framework for modeling memory, hereditary effects, and complex dynamics that are poorly captured by integer-order or commensurate fractional models.

Motivated by these considerations, this paper investigates the nonlinear, chaotic dynamics and coexisting attractors (Multistability) of a power system model within an incommensurate fractional-order framework. The obtained results provide deeper insight into the role of incommensurate fractional-order dynamics in power system stability and offer a more accurate theoretical basis for chaos analysis in modern power systems.

https://doi.org/10.3390/math14173164

2. Preliminaries

We provide a few critical preliminaries in relation to the non-integer calculus [18]:

Definition 1. *When applied to the function $h \in C^{\eta}(0,T]$, the Riemann–Liouville fractional-order integral operator κ is defined as follows:*

$$I^{\kappa}h(\mu) = \frac{1}{\Gamma(\kappa)}\int_0^{\mu}\frac{h(\sigma)}{(\mu-\sigma)^{(1-\kappa)}}d\sigma, \tag{1}$$

where $\kappa > 0$, $\eta \in \mathbb{N}$ and $T > 0$.

Definition 2. *The fractional-order κ differential operator of the function $h \in C^{\eta}(0,T]$ is as follows in the Caputo sense:*

$$D^{\kappa}h(\mu) = \begin{cases} \frac{1}{\Gamma(\eta-\kappa)}\int_0^{\mu}(t-\sigma)^{\eta-\kappa-1}h^{(\eta)}(\sigma)d\sigma, & \kappa \in (\eta-1,\eta), \\ h^{(\eta)}(\mu), & \kappa = \eta, \end{cases} \tag{2}$$

where $\kappa \in [\eta-1,\eta]$, $\eta \in \mathbb{N}$ and $T > 0$.

The incommensurate fractional-order dynamical system will now be analyzed [19]:

$$D^{\delta_i}\zeta_i = \varphi_i(\zeta_1,\zeta_2,\zeta_3), \qquad 1 \le i \le 3, \tag{3}$$

in which $\delta_i = \frac{m_i}{n_i}$ and $(m_i,n_i) = 1$ are positive integers, and m_i and n_i are positive integers between 0 and 1. L is the symbol used to represent the least common multiple of the values of m_i. The equilibrium point of the system (3) is denoted by $I \equiv (\zeta_1^*,\zeta_2^*,\zeta_3^*)$, while a minor perturbation from a fixed point is denoted by $\rho_i = \zeta_i - \zeta_i^*$ for $1 \le i \le 3$. After that,

$$\begin{aligned} D^{\delta_i}\rho_i &= D^{\delta_i}\zeta_i \\ &= \varphi_i(\zeta_1,\zeta_2,\zeta_3) = \varphi_i(\rho_1+\zeta_1^*,\rho_2+\zeta_2^*,\rho_3+\zeta_3^*) \\ &= \varphi_i(\zeta_1^*,\zeta_2^*,\zeta_3^*) + \rho_1\frac{\partial\varphi_i(p)}{\partial\zeta_1} + \rho_2\frac{\partial\varphi_i(p)}{\partial\zeta_2} + \rho_3\frac{\partial\varphi_i(p)}{\partial\zeta_3} + \text{higher ordered terms} \\ &\approx \rho_1\frac{\partial\varphi_i(p)}{\partial\zeta_1} + \rho_2\frac{\partial\varphi_i(p)}{\partial\zeta_2} + \rho_3\frac{\partial\varphi_i(p)}{\partial\zeta_3}. \end{aligned}$$

We acquire

$$D^{\delta_i}\rho_i \approx \zeta_1\frac{\partial\varphi_i(p)}{\partial\chi_1} + \rho_2\frac{\partial\varphi_i(p)}{\partial\zeta_2} + \rho_3\frac{\partial\varphi_i(p)}{\partial\zeta_3}. \tag{4}$$

The system described in (4) is equivalent to

$$\begin{pmatrix} D^{\delta_1}\rho_1 \\ D^{\delta_2}\rho_2 \\ D^{\delta_3}\rho_3 \end{pmatrix} = K\begin{pmatrix} D^{\delta_1}\rho_1 \\ D^{\delta_2}\rho_2 \\ D^{\delta_3}\rho_3 \end{pmatrix}, \tag{5}$$

where K is the Jacobian matrix evaluated at point I, which is defined as

$$K = \begin{pmatrix} \partial_1\varphi_1(I) & \partial_2\varphi_1(I) & \partial_3\varphi_1(I) \\ \partial_1\varphi_2(I) & \partial_2\varphi_2(I) & \partial_3\varphi_2(I) \\ \partial_1\varphi_3(I) & \partial_2\varphi_3(I) & \partial_3\varphi_3(I) \end{pmatrix}$$

Define

$$D(\lambda) = diag([\lambda^{L\delta_1}\lambda^{L\delta_2}\lambda^{L\delta_3}]) - K. \tag{6}$$

https://doi.org/10.3390/math14173164

If every root of the equation $\det(D(\lambda)) = 0$ meets the criterion $|\arg(\lambda)| > \frac{\pi}{2L}$, then the linear system (5) is asymptotically stable [20].

The quantity
$$IMFOS = \frac{\pi}{2L} - \min_i |\arg(\lambda_i)|,$$
provides a measure of the instability of the equilibrium point in an incommensurate fractional-order system. According to [19], the condition $IMFOS \geq 0$ is a necessary condition for the occurrence of chaotic dynamics. However, this condition alone is insufficient to establish chaos; additional numerical diagnostics, such as the Lyapunov spectrum, are required for confirmation.

3. Mathematical Model of the Power System

Synchronous generators, although they serve as the principal energy source in power systems, exert a considerable influence on dynamic fluctuations. In [13,14], Shun-Chang Chang examines a power system model with three synchronous generators and a resistive load configuration, as illustrated in Figure 1. The subsequent equations delineate the nonlinear dynamics of the examined power system, according to [21,22]:

$$\begin{aligned}
\dot{\delta}_1 &= \omega_1, &\text{(7a)}\\
M_1\dot{\omega}_1 &= -D_1\omega_1 + P_1 - F_{12}\sin(\delta_1 - \delta_2) - F_{13}\sin(\delta_1 - \delta_3), &\text{(7b)}\\
\dot{\delta}_2 &= \omega_2, &\text{(7c)}\\
M_2\dot{\omega}_2 &= -D_2\omega_2 + P_2 - F_{21}\sin(\delta_2 - \delta_1) - F_{23}\sin(\delta_2 - \delta_3), &\text{(7d)}\\
\dot{\delta}_3 &= \omega_3, &\text{(7e)}\\
M_3\dot{\omega}_3 &= -D_3\omega_3 + P_3 - F_{31}\sin(\delta_3 - \delta_1) - F_{32}\sin(\delta_3 - \delta_2). &\text{(7f)}
\end{aligned}$$

The above system describes a classical third-order swing equation model governing the rotor angle dynamics of a three-machine power system. In order to reduce the complexity while preserving the essential nonlinear behavior, a reduced-order formulation is introduced based on standard simplifying assumptions.

The dynamic analysis of the three-machine system is subsequently examined in a peculiar situation, in which the swing equations are employed. It is presumed that Machine-1 has an inertia that is substantially greater than that of

$$M_1 = \frac{\bar{M}}{\varepsilon}, \qquad \varepsilon \ll 1. \tag{8}$$

Additionally, it is presumed that the transmission line connecting Machines 2 and 3 is shorter than the other transmission lines. The external power input of Machine1 is also assumed to be proportionately substantial and is delineated as

$$P_1 = \frac{\bar{P}_1}{\varepsilon}. \tag{9}$$

These assumptions allow the system to be expressed in a singular perturbation framework, where Machine 1 acts as a fast/strongly dominant subsystem, enabling model reduction.

The conservative swing equations that govern the dynamics of the three-machine system can be constructed appropriately based on these assumptions. The dynamic behavior is given by:

$$\dot{\delta}_1 = \omega_1, \tag{10a}$$
$$M_1\dot{\omega}_1 = -D_1\omega_1 + P_1 - F_{12}\sin(\delta_1 - \delta_2) - F_{13}\sin(\delta_1 - \delta_3), \tag{10b}$$
$$\dot{\delta}_2 = \omega_2, \tag{10c}$$
$$M_2\dot{\omega}_2 = -D_2\omega_2 + P_2 - F_{21}\sin(\delta_2 - \delta_1) - F_{23}\sin(\delta_2 - \delta_3), \tag{10d}$$
$$\dot{\delta}_3 = \omega_3, \tag{10e}$$
$$M_3\dot{\omega}_3 = -D_3\omega_3 + P_3 - F_{31}\sin(\delta_3 - \delta_1) - F_{32}\sin(\delta_3 - \delta_2). \tag{10f}$$

Under the above assumptions, the system is further simplified by expressing the rotor angle of generator 1 in terms of generators 2 and 3, leading to a reduced-order model.

According to Refs. [21,22], the rotor angle of the first generator can be articulated as

$$\delta_1 = -\mu_2\delta_2 - \mu_3\delta_3, \tag{11}$$

where $\mu_2 = \dfrac{M_2}{\bar{M}_1}$ and $\mu_3 = \dfrac{M_3}{\bar{M}_1}$.

By substituting Equation (11) into Equation (10a) through (10f), an autonomous reduced-order dynamical system for δ_2, δ_3, ω_2, and ω_3 is derived.

This transformation eliminates the fast variables δ_1 and ω_1, yielding a four-dimensional reduced-order system that retains the essential nonlinear coupling structure of the original model.

$$\dot{\delta}_2 = \omega_2, \tag{12a}$$
$$\dot{\omega}_2 = -D_2\omega_2 + \bar{\alpha}_2 - \beta_{21}\sin[\delta_2(1 + \varepsilon\mu_2) + \varepsilon\mu_3\delta_3] - \beta_{23}\sin(\delta_2 - \delta_3), \tag{12b}$$
$$\dot{\delta}_3 = \omega_3, \tag{12c}$$
$$\dot{\omega}_3 = -D_3\omega_3 + \bar{\alpha}_3 - \beta_{31}\sin[\delta_3(1 + \varepsilon\mu_3) + \varepsilon\mu_2\delta_2] - \beta_{32}\sin(\delta_3 - \delta_2). \tag{12d}$$

where $\bar{\alpha}_2 = \dfrac{P_2}{M_2}$, $\beta_{21} = \dfrac{F_{21}}{M_2}$, $\beta_{23} = \dfrac{F_{23}}{M_2}$, $\bar{\alpha}_3 = \dfrac{P_3}{M_3}$, $\beta_{31} = \dfrac{F_{31}}{M_3}$, and $\beta_{32} = \dfrac{F_{32}}{M_3}$. For simplicity and without loss of generality, the parameter ε is set to zero, which allows Equation (12a–d) to be further simplified as follows:

$$\dot{\delta}_2 = \omega_2, \tag{13a}$$
$$\dot{\omega}_2 = -D_2\omega_2 + \bar{\alpha}_2 - \beta_{21}\sin(\delta_2) - \beta_{23}\sin(\delta_2 - \delta_3), \tag{13b}$$
$$\dot{\delta}_3 = \omega_3, \tag{13c}$$
$$\dot{\omega}_3 = -D_3\omega_3 + \bar{\alpha}_3 - \beta_{31}\sin(\delta_3) - \beta_{32}\sin(\delta_3 - \delta_2). \tag{13d}$$

This simplification preserves the essential nonlinear interactions while reducing analytical complexity, which is suitable for bifurcation and chaos analysis.

In accordance with [21,22], the term $\bar{\alpha}_k$ can be expressed as

$$\bar{\alpha}_k = \bar{P}_k - K_f\omega_k, \qquad k = 2, 3. \tag{14}$$

where $\bar{P}_k$ denotes the constant real power input, $K_f = \dfrac{L_k}{M_k}$, and L_k represents the load–frequency coefficient.

Substituting Equation (14) into Equation (13a–d), the system can be rewritten as:

$$\dot{\delta}_2 = \omega_2, \tag{15a}$$
$$\dot{\omega}_2 = -D_2\omega_2 + \bar{P}_2 - K_f\omega_2 - \beta_{21}\sin(\delta_2) - \beta_{23}\sin(\delta_2 - \delta_3), \tag{15b}$$
$$\dot{\delta}_3 = \omega_3, \tag{15c}$$
$$\dot{\omega}_3 = -D_3\omega_3 + \bar{P}_3 - K_f\omega_3 - \beta_{31}\sin(\delta_3) - \beta_{32}\sin(\delta_3 - \delta_2). \tag{15d}$$

Letting $y_1 = \delta_2$, $y_2 = \omega_2$, $y_3 = \delta_3$, and $y_4 = \omega_3$ be the state variables, the state-space representation is obtained.

$$\begin{cases} \dot{y_1} = y_2, \\ \dot{y_2} = p_2 - (D_2 + K_f)y_2 - \beta_{21}\sin(y_1) - \beta_{23}\sin(y_1 - y_3), \\ \dot{y_3} = y_4, \\ \dot{y_4} = p_3 - (D_3 + K_f)y_4 - \beta_{31}\sin(y_3) - \beta_{32}\sin(y_3 - y_1). \end{cases} \tag{16}$$

The $y_i, (i = 1, \dots, 4)$ are the state variables of the reduced-order swing equation model, where rotor angle differences are measured with respect to generator 1 as the reference machine, and angular speed deviations characterize the system dynamics. All the parameters in system (16) are mentioned in Table 1.

Table 1. System parameter values (16).

Parameter	Value	Description
β_{21}	-2	Coupling coefficient between generator 1 and generator 2
β_{23}	-1	Coupling coefficient between generator 2 and generator 3
β_{31}	-1	Coupling coefficient between generator 3 and generator 1
β_{32}	-1	Coupling coefficient between generator 3 and generator 2
D_2	0.2	Damping coefficient of generator 2
D_3	0.5	Damping coefficient of generator 3
p_2	0.3	Mechanical input power of generator 2
p_3	0.5	Mechanical input power of generator 3
K_f	0.008	Load-frequency coefficient

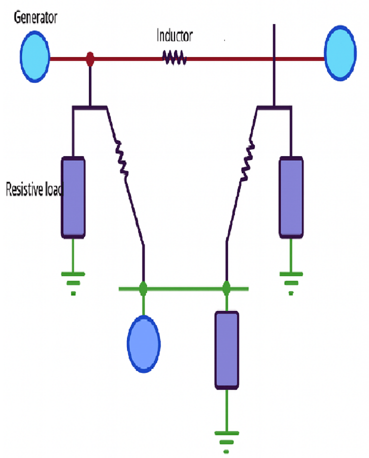

Figure 1. Power system diagrams.

Understanding the dynamic features of power systems requires examination of interconnected systems using synchronous motors as primary components.

This study will employ incommensurate fractional-order derivatives on the system (16) and examine various dynamic behaviors through analytical and numerical methods. The use of incommensurate fractional orders allows different state variables to possess distinct memory characteristics and dynamic responses. In practical power systems, rotor-angle deviations and frequency deviations may be influenced by different physical processes, damping mechanisms, and energy storage effects. Consequently, assigning different fractional orders to the state variables provides a more flexible framework for capturing heterogeneous memory effects and complex dynamical behavior than the commensurate case, where all states share the same fractional order. The fractional-order variant of the preceding power system is represented by the following equations:

$$\begin{cases} D_t^{q_1} y_1 = y_2, \\ D_t^{q_2} y_2 = p_2 - (D_2 + K_f) y_2 - \beta_{21} sin(y_1) - \beta_{23} sin(y_1 - y_3), \\ D_t^{q_3} y_3 = y_4, \\ D_t^{q_4} y_4 = p_3 - (D_3 + K_f) y_4 - \beta_{31} sin(y_3) - \beta_{32} sin(y_3 - y_1). \end{cases} \tag{17}$$

In this context, D^q denotes the q-order Caputo differential operator, where $0 < q_i \leq 1$ for $i = 1,2,3,4$, representing the derivative orders of the state variables y_i for $i = 1,2,3,4$. If the values q_i (for $i = 1,2,3,4$) are distinct, the fractional-order system (17) is deemed incommensurate. Different fractional orders are introduced to model heterogeneous memory effects. Since the four state variables describe different physical mechanisms of the power system, their memory characteristics are not necessarily identical. Therefore, assigning different fractional orders provides a more flexible and realistic representation. Diethelm utilized the predictor–corrector technique, an advanced iteration of the Adams–Bashforth–Moulton algorithm, for numerical simulations of fractional differential equations defined by the Caputo approach [23].

The Jacobian matrix of the system (17) is given by:

$$K = \begin{pmatrix} 0 & 1 & 0 & 0 \\ -\beta_{21}\cos(y_1) - \beta_{23}\cos(y_1 - y_3) & -(D_2 + K_f) & \beta_{23}\cos(y_1 - y_3) & 0 \\ 0 & 0 & 0 & 1 \\ \beta_{32}\cos(y_1 - y_3) & 0 & -\beta_{31}\cos(y_3) - \beta_{32}\cos(y_3 - y_1) & -(D_3 + K_f) \end{pmatrix}. \tag{18}$$

The system (16) has two points of equilibrium: the first is the origin $Y_0 = (0,0,0,0)$ and the second is $Y_1 = (K\pi, 0, m\pi, 0)$, where k and m are both integers. The system (16) has an equilibrium point $Y_1 = (-0.151, 0, -0.524, 0)$, which can be found numerically by using the parameter values in Table 1. Its eigenvalues are $(-2.0093, -1.3577, 1.7241, 0.9269)$, which means it is a saddle point and is thus unstable.

4. Chaotic Analysis

4.1. Dynamic Analysis Versus the Fractional Orders

This section examines the onset of chaotic dynamics in the incommensurate-order power system through both analytical and numerical approaches. The analysis includes bifurcation diagrams, Lyapunov exponent computations, and phase-space portraits presented in two- and three-dimensional projections. All simulations are conducted using the parameter values listed in Table 1 and the initial condition (15, 0.3, 0.4, 0).

To verify the chaotic behavior of the proposed incommensurate fractional-order system, the Lyapunov spectrum is computed for several fractional-order configurations. The obtained results are summarized in Table 2. The maximum Lyapunov exponent (MLE) is positive for all considered cases, confirming the presence of chaotic dynamics.

The bifurcation diagrams and Lyapunov exponent spectra are analyzed jointly to provide a consistent characterization of the system dynamics.

Table 2. Maximum Lyapunov exponent (MLE) for different fractional-order configurations.

q_1	q_2	q_3	q_4	MLE
0.99	1.00	1.00	1.00	0.049020
1.00	0.98	1.00	1.00	0.001262
1.00	1.00	0.98	1.00	0.018265
1.00	1.00	1.00	0.90	0.005929

We evaluate the stability of an incommensurate system (17) by generating bifurcation diagrams for four distinct scenarios: $q_1 \in (0.9, 1), q_i = 1$ with $i = 2, 3, 4$; $q_2 \in (0.9, 1), q_i = 1$ with $i = 1, 3, 4$; $q_3 \in (0.7, 1), q_i = 1$ with $i = 1, 2, 4$; and $q_4 \in (0.7, 1), q_i = 1$ with $i = 1, 2, 3$.

This combined analysis allows a clear identification of the transition mechanism from regular periodic motion to chaos induced by variations in the fractional-order parameters.

When $q_1, q_2 < 0.94$ and $q_3, q_4 < 0.80$, it is evident that the equilibrium point of system (17) is asymptotically stable. When $q_1, q_2 \in (0.94, 1)$ and $q_3, q_4 \in (0.8, 1)$, the incommensurate system began to destabilize, resulting in a transition from periodic motion to chaos.

The incommensurate system (17) demonstrates chaotic behavior for $q_1, q_2 \in (0.98, 1)$, $q_3 \in (0.81, 1)$, and $q_4 \in (0.86, 1)$ as evidenced by the Lyapunov exponent plots in Figures 2b–5b.

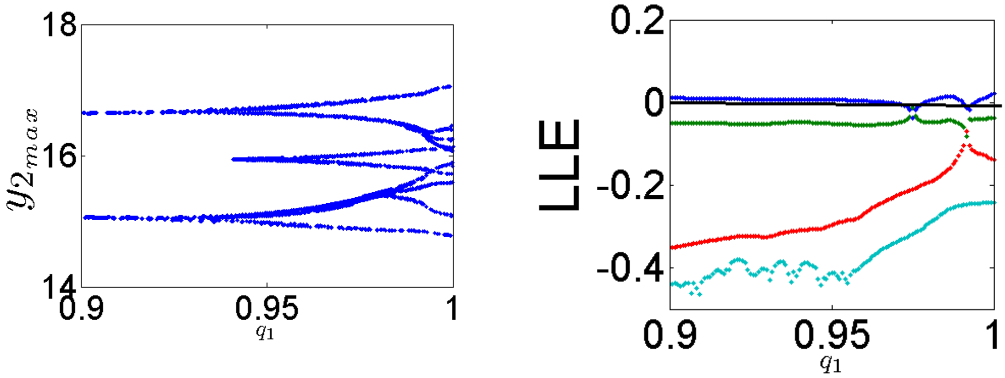

(**a**) (**b**)

Figure 2. (**a**) Bifurcation diagram; (**b**) Lyapunov exponents of the incommensurate system (17) with varying $q_1 \in (0.9, 1)$, $q_2 = q_3 = q_4 = 1$, using the parameter set reported in Table 1 and initial conditions $(15, 0.3, 0.4, 0)$.

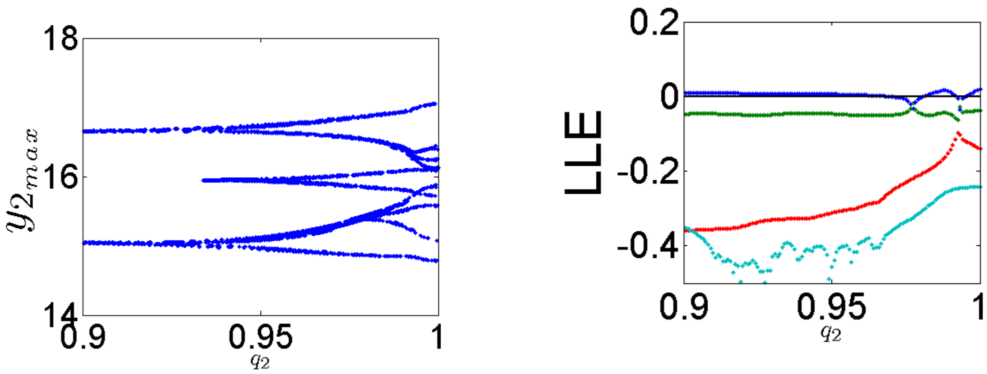

(**a**) (**b**)

Figure 3. (**a**) Bifurcation diagram; (**b**) Lyapunov exponents of the incommensurate system (17) for $q_2 \in (0.9, 1)$, with $q_1 = q_3 = q_4 = 1$, utilizing system parameters selected from Table 1 and specified initial conditions.

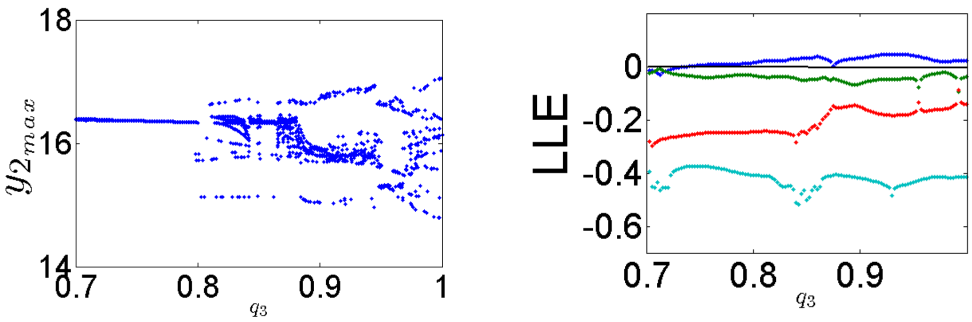

(**a**) (**b**)

Figure 4. (**a**) Bifurcation diagram and (**b**) Lyapunov exponents of the incommensurate system (17) in relation to $q_3 \in (0.7, 1)$, where $q_1 = q_2 = q_4 = 1$. In accordance with Table 1, the initial conditions are established as $(15, 0.3, 0.4, 0)$. System parameters are selected accordingly.

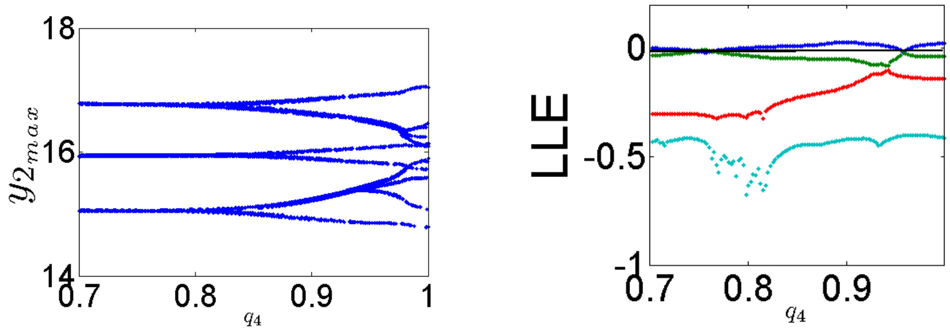

(**a**) (**b**)

Figure 5. (**a**) Bifurcation diagram; (**b**) Lyapunov exponents of the incommensurate system (17) for $q_4 \in (0.7, 1)$, with $q_1 = q_2 = q_3 = 1$, and initial conditions $(15, 0.3, 0.4, 0)$, utilizing system parameters selected from Table 1.

From Figures 2–5, it is observed that decreasing the fractional-order parameters leads to a reduction in system complexity, where the system initially exhibits periodic behavior, followed by transitions into chaotic dynamics. The corresponding Lyapunov exponent plots confirm this behavior, as positive values of the largest Lyapunov exponent coincide with the chaotic regions identified in the bifurcation diagrams, ensuring consistency between both diagnostic tools.

To further validate these results, phase portraits are used to visualize the qualitative evolution of the system trajectories under different fractional-order values.

The phase portraits of the incommensurate system (17) on the $y_1 - y_2$ plane are depicted in Figure 6 for a variety of values of q_1, q_2, q_3, and q_4:

* For the incommensurate order q_1, with $(q_2, q_3, q_4) = (1, 1, 1)$ fixed, system (17) converges to a limit cycle at $q_1 = 0.90$, while chaotic dynamics are observed for $q_1 = 0.95$ and $q_1 = 0.99$ (Figure 6a).
* Keeping $(q_1, q_3, q_4) = (1, 1, 1)$ unchanged and varying q_2, the system approaches a limit cycle at $q_2 = 0.90$. As q_2 increases to 0.95 and 0.99, the dynamics evolve into chaotic behavior (Figure 6b).
* With $(q_1, q_2, q_4) = (1, 1, 1)$ fixed, decreasing q_3 to 0.70 drives the system toward the equilibrium point. In contrast, chaotic dynamics emerge for $q_3 = 0.90$ and $q_3 = 0.99$ (Figure 6c).

* Finally, for $(q_1, q_2, q_3) = (1, 1, 1)$, the system settles onto a limit cycle at $q_4 = 0.70$, whereas chaotic behavior is obtained at $q_4 = 0.90$ and $q_4 = 0.98$ (Figure 6d). The corresponding three-dimensional phase portraits are presented in Figure 7, showing the system trajectories in the $y_1 - y_2 - y_3$, $y_1 - y_2 - y_4$, and $y_2 - y_3 - y_4$ projections.

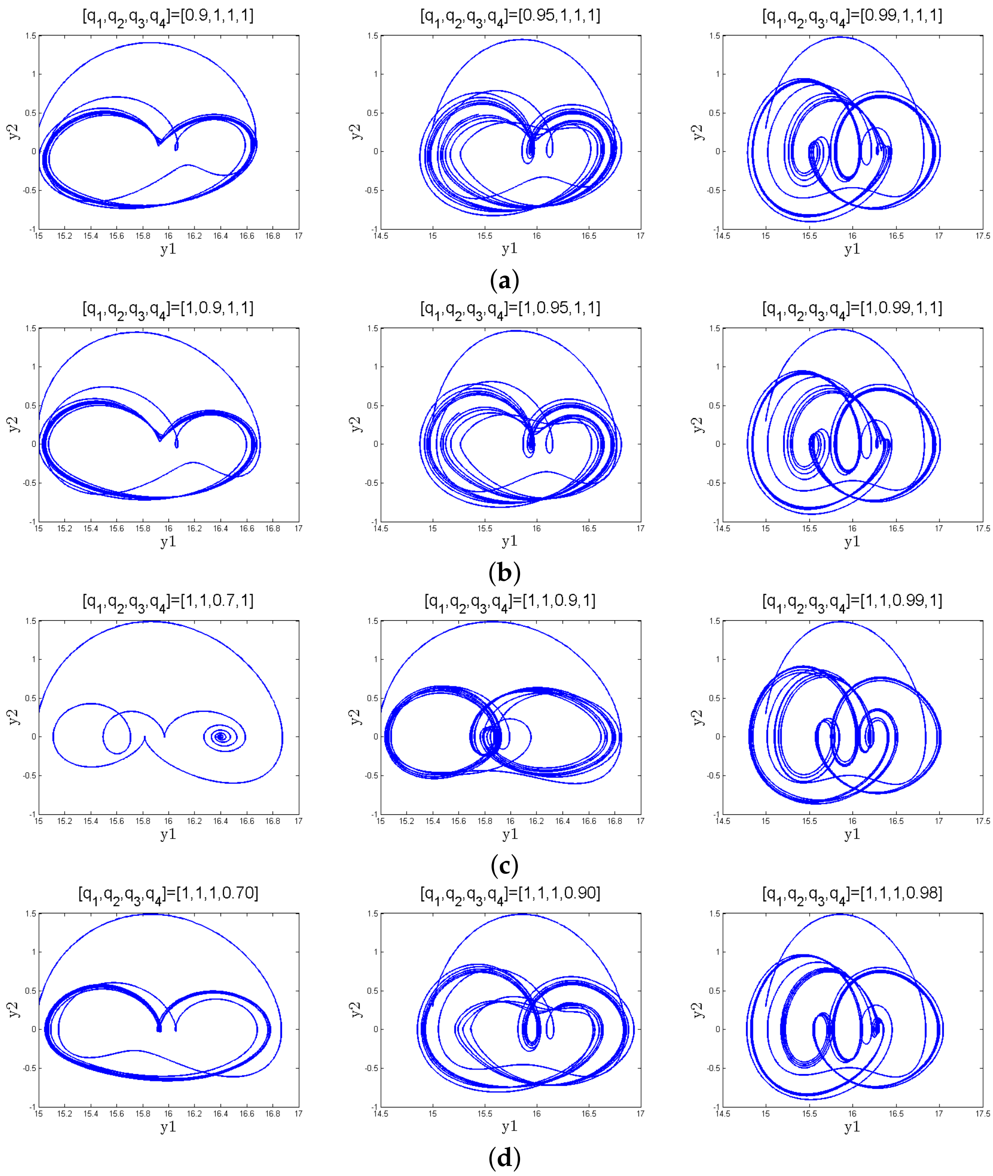

Figure 6. Phase portraits of an incommensurate system (17) are obtained by selecting the system parameters from Table 1 and establishing the starting conditions to ensure that $(15, 0.3, 0.4, 0)$. The factors were also altered as a result of the changes to (**a**) q_1, (**b**) q_2, (**c**) q_3, and (**d**) q_4.

These results demonstrate that incommensurate fractional-order parameters play a crucial role in controlling the system's dynamical behavior, with specific ranges of the fractional orders inducing transitions from stable periodic motion to chaotic regimes. The agreement between bifurcation diagrams, Lyapunov exponents, and phase portraits confirms the reliability of the numerical analysis.

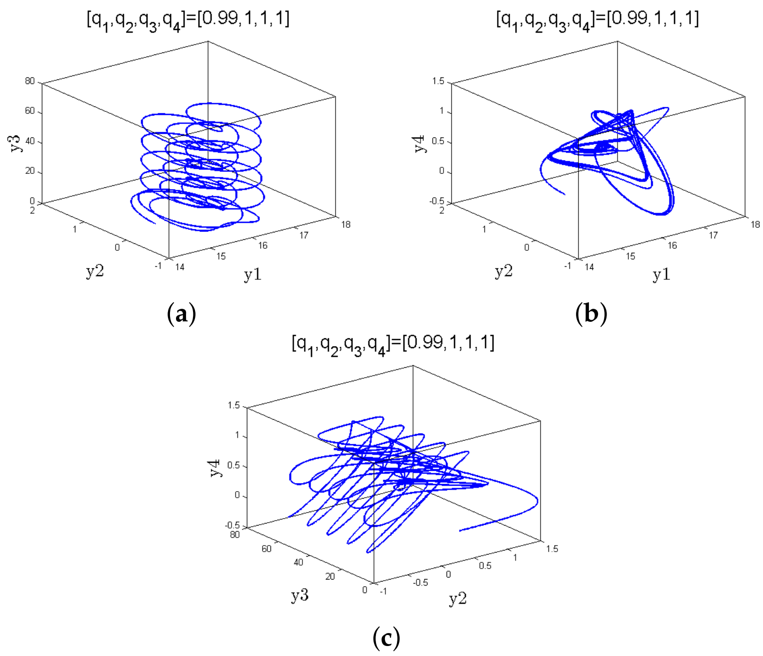

Figure 7. Phase portraits on 3D projection of incommensurate system (17) with taking system parameters selecting in Table 1 and initial conditions $(15, 0.3, 0.4, 0)$ by: (**a**) on y_1, y_2, y_3 plan, (**b**) on y_1, y_2, y_4 plan and (**c**) on y_2, y_3, y_4 plan.

Furthermore, the stability of an incommensurate order power system was studied theoretically by using the method in Section 2. Consider the system (17). The Lyapunov exponent is positive for $q_1, q_2 = 0.98, q_3 = q_4 = 1$ (see Figures 2b and 3b) and for $q_3, q_4 = 0.96, q_1 = q_2 = 1$ (see Figures 4b and 5b). Now consider the following cases:

* $q_1 = 49/50, q_2 = q_3 = q_4 = 1$. Therefore $L = lcm(50, 1, 1, 1) = 50$.

  Since
  $$\Delta(\lambda) = diag(\lambda^{49}\lambda^{50}\lambda^{50}\lambda^{50}) - K(Y_1),$$
  $$det(\Delta(\lambda)) = \lambda^{199} + 0.716\lambda^{149} - 1.88\lambda^{99} - 0.414\lambda^{49} - 2.97\lambda^{100} - 1.51\lambda^{50} + 4.92.$$

  A positive IMFOS satisfies only the necessary condition for chaos. The existence of chaotic dynamics is confirmed numerically through the Lyapunov spectrum and phase portraits.
  The IMFOS of the system is:
  $$\frac{\pi}{100} - 0.00 = 0.0327 > 0$$

  Though IMFOS > 0, the system shows chaotic behavior. This is confirmed numerically in Figure 2b.

* $q_2 = 49/50, q_1 = q_3 = q_4 = 1$. Therefore $L = LCM(1, 50, 1, 1) = 50$. Since $\Delta(\lambda) = diag(\lambda^{50}\lambda^{49}\lambda^{50}\lambda^{50}) - K(Y_1)$, $det(\Delta(\lambda)) = \lambda^{199} + 0.716\lambda^{149} - 1.88\lambda^{99} - 0.414\lambda^{49} - 2.97\lambda^{100} - 1.51\lambda^{50} + 4.92$. The IMFOS of the system is:
  $$\frac{\pi}{100} - 0.00 = 0.0327 > 0$$

  Though IMFOS > 0, the system shows chaotic behavior. This is confirmed numerically in Figure 3b.

* $q_3 = 48/50, q_1 = q_2 = q_4 = 1$. Therefore $M = LCM(1,1,50,1) = 50$. Since $\Delta(\lambda) = diag(\lambda^{50}\lambda^{50}\lambda^{48}\lambda^{50}) - J(E_1)$, $det(\Delta(\lambda)) = \lambda^{198} + 0.716\lambda^{148} - 1.99\lambda^{100} - 2.86\lambda^{98} - 0.414\lambda^{50} - 1.51\lambda^{48} + 4.92$. The IMFOS of the system is:

$$\frac{\pi}{100} - 0.00 = 0.0327 > 0$$

  Though IMFOS > 0, the system shows chaotic behavior. This is confirmed numerically in Figure 4b.
* $q_4 = 47/50, q_1 = q_2 = q_3 = 1$. Therefore $M = LCM(1,1,1,50) = 50$. Since $\Delta(\lambda) = diag(\lambda^{50}\lambda^{50}\lambda^{50}\lambda^{47}) - J(E_1)$, $det(\Delta(\lambda)) = \lambda^{197} + 0.508\lambda^{150} - 1.88\lambda^{100} + 0.208\lambda^{147} - 1.92\lambda^{50} - 2.97\lambda^{97} + 4.92$. The IMFOS of the system is:

$$\frac{\pi}{100} - 0.00 = 0.0327 > 0$$

  Though IMFOS > 0, the system shows chaotic behavior. This is confirmed numerically in Figure 5b.

As a result, it is possible to infer that the fractional variant of the power system exhibits chaotic behavior when subjected to a variety of incommensurate fractional orders. Each system has its own chaotic ranges. For the incommensurate order q_3, the system can exhibit chaos at the lowest fractional order value of $q3 = 0.81$, with $q_1 = q_2 = q_4 = 1$.

4.2. Dynamic Analysis Versus the Parameter of Load-Frequency Coefficient K_f

This section examines the existence of chaotic behavior in the incommensurate order power system using numerical tools, such as Lyapunov exponents and bifurcation diagrams. Table 1 is utilized to ascertain the system parameters and initial circumstances, which are $(15, 0.3, 0.4, 0)$.

Figures 8a–11a present bifurcation diagrams for four distinct scenarios: $[q_1, q_2, q_3, q_4] = [0.99, 1, 1, 1]$, $[q_1, q_2, q_3, q_4] = [1, 0.99, 1, 1]$, $[q_1, q_2, q_3, q_4] = [1, 1, 1, 0.98]$, and $[q_1, q_2, q_3, q_4] = [1, 1, 1, 0.98]$.

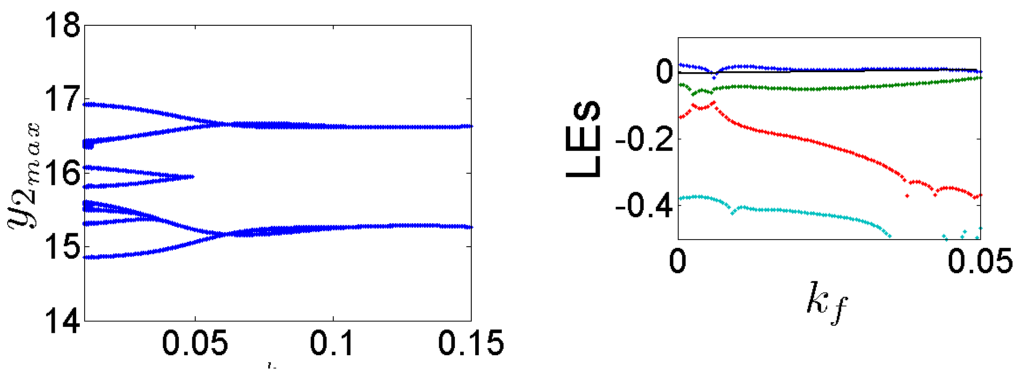

(**a**) (**b**)

Figure 8. (**a**) Bifurcation diagram of the considered system, (**b**) corresponding Lyapunov exponent spectrum of the incommensurate fractional-order model for $K_f \in (0, 0.15)$, with fractional orders $[q_1, q_2, q_3, q_4] = [0.99, 1, 1, 1]$. The remaining system parameters are taken from Table 1. The initial state vector is selected as $(15, 0.3, 0.4, 0)$.

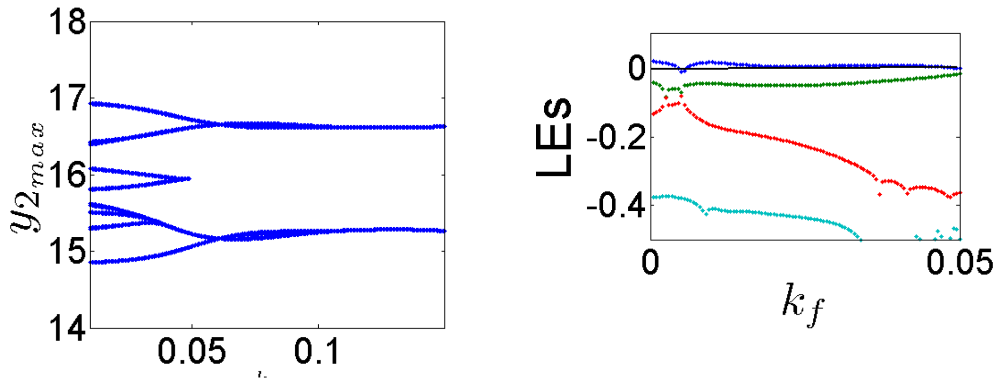

(**a**) (**b**)

Figure 9. Panels (**a**,**b**) present the bifurcation structure and the associated Lyapunov exponent spectrum of the incommensurate system (17) as K_f varies within $(0, 0.15)$. The parameter values are adopted from Table 1. The initial conditions are set to $(15, 0.3, 0.4, 0)$.

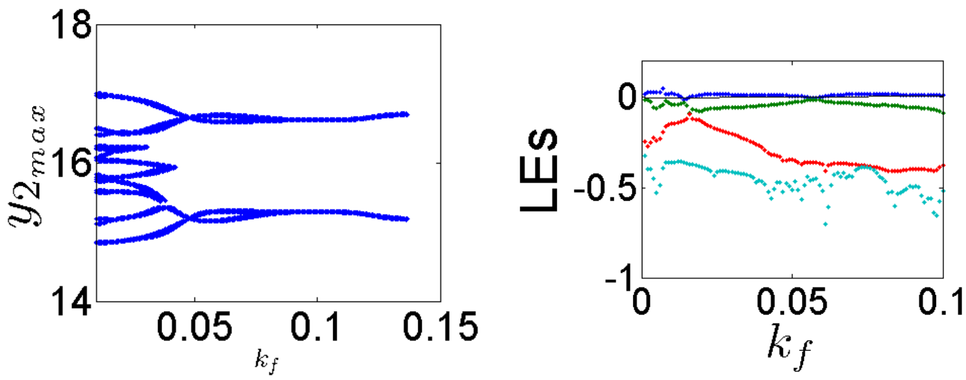

(**a**) (**b**)

Figure 10. (**a**) Bifurcation structure and (**b**) associated Lyapunov exponents of system (17) for $K_f \in (0, 0.15)$ with $[q_1, q_2, q_3, q_4] = [1, 1, 0.99, 1]$. The parameters are from Table 1, and the starting state is $(15, 0.3, 0.4, 0)$.

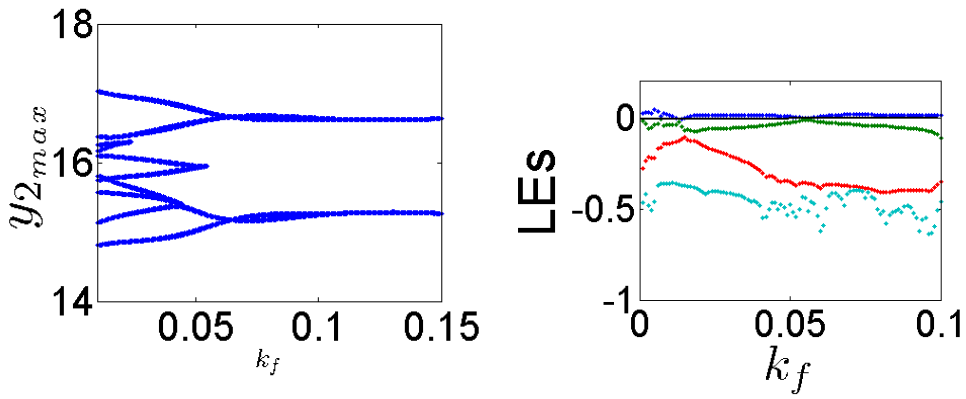

(**a**) (**b**)

Figure 11. (**a**) Bifurcation diagram, (**b**) Lyapunov exponents of the incommensurate system (17) for $K_f \in (0, 0.15)$, with parameters $[q_1, q_2, q_3, q_4] = [1, 1, 1, 0.98]$, as specified in Table 1, and initial conditions $(15, 0.3, 0.4, 0)$.

The equilibrium point of system (17) is asymptotically stable when $k_f > 0.05$ throughout the four scenarios, indicating the absence of chatter vibration.

As K_f decreases within the interval $(0, 0.05)$, the incommensurate system begins to lose stability, transitioning from periodic motion to chaos. The plots of Lyapunov exponents in Figures 8b–11b indicate that the incommensurate system (17) exhibits chaotic behavior for $k_f \in (0, 0.015)$ in the first case, $k_f \in (0, 0.0145)$ in the second case, $k_f \in (0, 0.011)$ in the third case, and $k_f \in (0, 0.010)$ in the fourth case. The resultant chatter vibrations were sufficiently intense to cause a voltage failure in the power supply.

5. Multistability and Coexisting Attractors

The coexistence of multiple attractors and multistability in incommensurate fractional-order systems has attracted considerable attention due to its important implications for nonlinear dynamical behavior. In such systems, different initial conditions may lead to distinct long-term responses under identical parameter settings. Throughout this section, the initial conditions are chosen as $(y_1(0), 0.3, 0.4, 0)$ with $y_1(0) \in \{15, 8, 2, -3, -9, -16\}$. These six initial values are distinguished by different colors in all corresponding figures.

Figure 12 presents the bifurcation diagram of the incommensurate fractional-order power system (17) as the fractional order q_1 varies, while the remaining parameters are fixed according to Table 1. The repeated bifurcation structures corresponding to different initial conditions clearly demonstrate the multistability of the proposed system. Moreover, each branch exhibits transitions among stable, periodic, and chaotic regimes, as illustrated in the enlarged view of Figure 9.

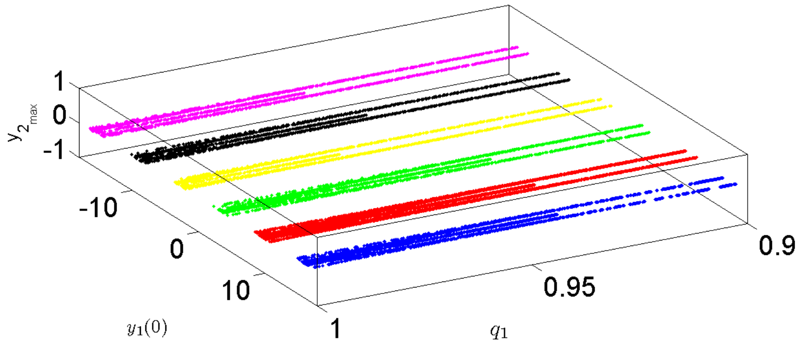

Figure 12. Coexisting bifurcation diagrams of system (17) obtained by varying the fractional order q_1. The remaining parameters are given in Table 1. The initial conditions are $(y_1(0), 0.3, 0.4, 0)$ with $y_1(0) \in \{15, 8, 2, -3, -9, -16\}$. Different colors correspond to different initial values.

To further illustrate the multistable behavior, the corresponding phase portraits are shown in Figure 13 for three representative values of the fractional order, namely $q_1 = 0.90$, 0.95, and 0.99. The coexistence of distinct trajectories generated from different initial conditions confirms that the incommensurate fractional-order power system possesses multiple coexisting dynamical states. Furthermore, the transition from periodic motion to chaotic dynamics follows a period-doubling bifurcation scenario.

Figure 14 further investigates the influence of the incommensurate fractional orders by varying each of q_1, q_2, q_3, and q_4 individually while keeping the remaining orders fixed. The obtained phase portraits reveal the coexistence of multiple chaotic dynamics under identical system parameters but different initial conditions, highlighting the strong sensitivity of the system dynamics to the initial state.

To further examine the influence of nearby initial conditions, coexisting bifurcation diagrams are computed for $q_3 \in [0.7, 1]$. Three closely spaced initial conditions, namely $(14, 0.3, 0.4, 0)$, $(15, 0.3, 0.4, 0)$, and $(16, 0.3, 0.4, 0)$, are considered. As shown in Figure 15, similar as well as distinct bifurcation structures are obtained, confirming the persistence of multistability even under small perturbations of the initial state. The corresponding coexisting chaotic dynamics and time series for $[q_1, q_2, q_3, q_4] = [1, 1, 0.99, 1]$ are presented in Figure 16.

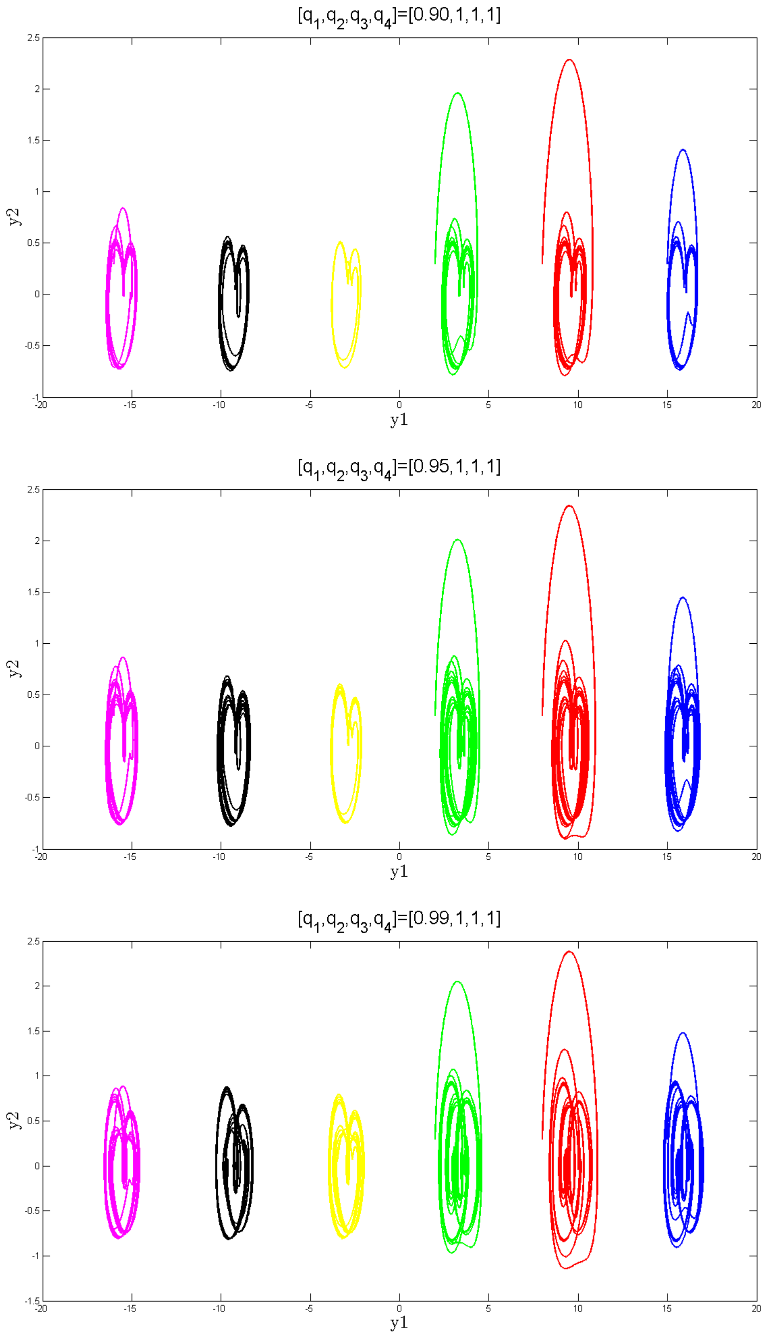

Figure 13. Coexisting dynamical behaviors of system (17) for different values of q_1. The system parameters are listed in Table 1, while the initial conditions are $(y_1(0), 0.3, 0.4, 0)$ with $y_1(0) \in \{15, 8, 2, -3, -9, -16\}$. Different colors denote different initial values.

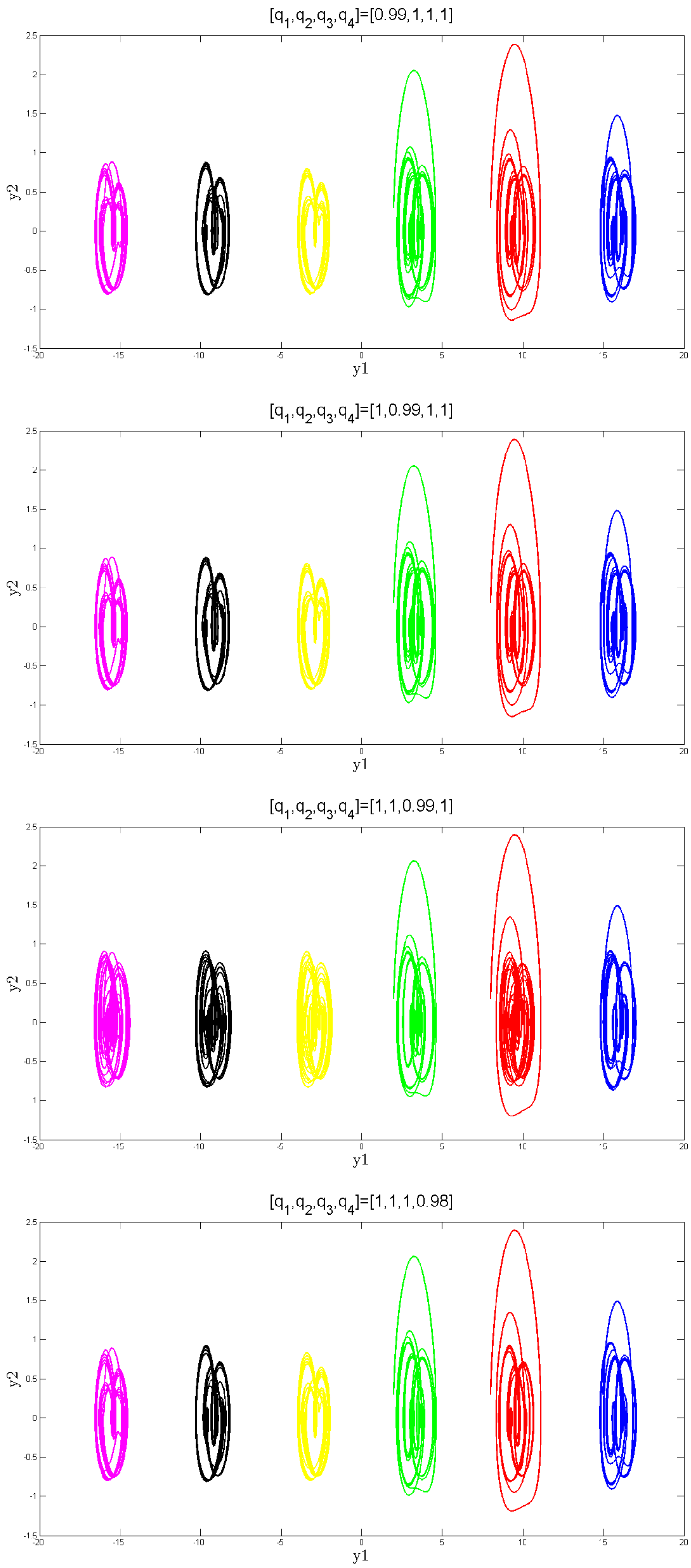

Figure 14. Coexisting dynamical behaviors of system (17) for different incommensurate fractional orders. The parameters are taken from Table 1. The initial conditions are $(y_1(0), 0.3, 0.4, 0)$ with $y_1(0) \in \{15, 8, 2, -3, -9, -16\}$. Different colors indicate different initial values.

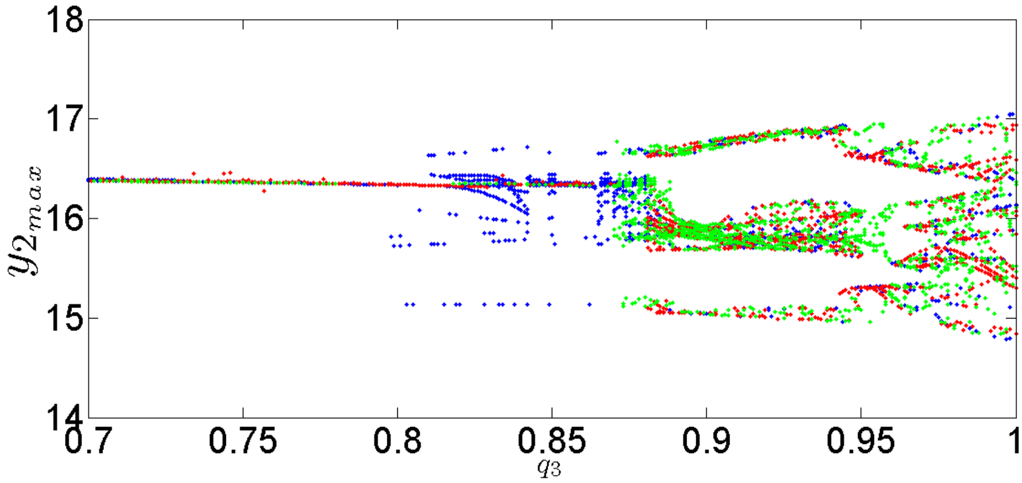

Figure 15. Coexisting bifurcation structures of the incommensurate fractional-order system (17). The settings for the system come from Table 1. The starting conditions are given as $(y_1(0), 0.3, 0.4, 0)$, where $y_1(0)$ is either 14, 15, or 16. The three instances are shown with green, blue, and red lines.

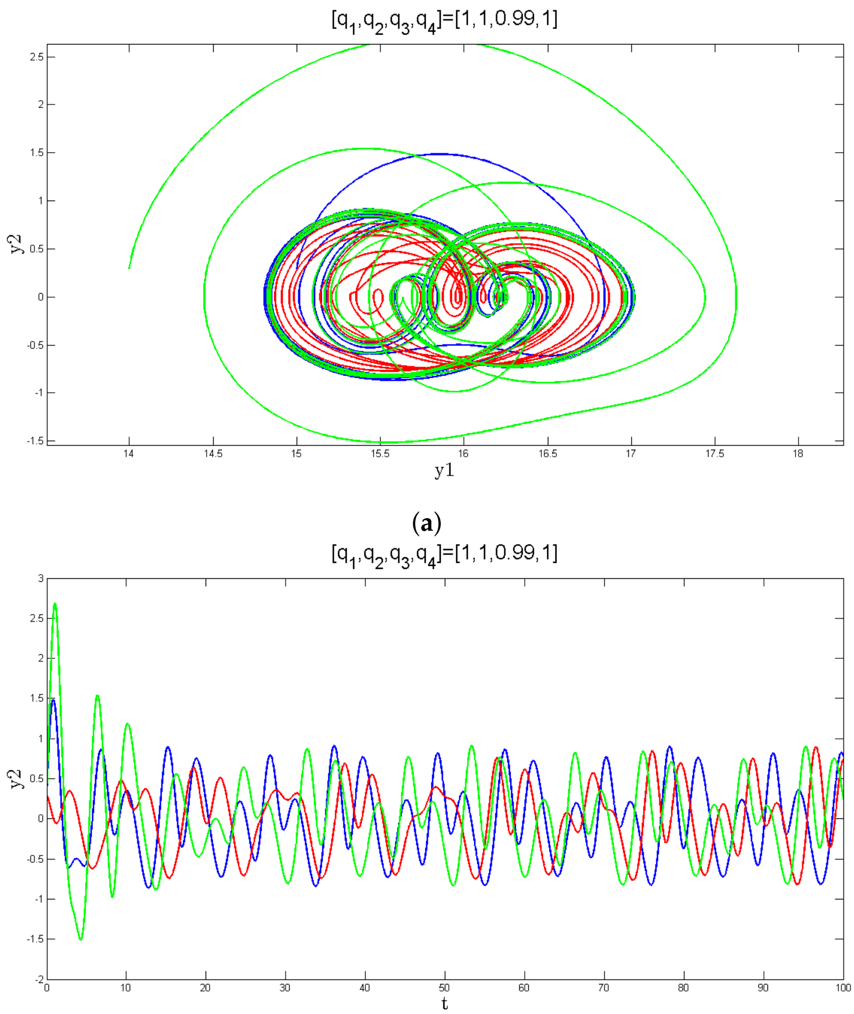

(**a**)

(**b**)

Figure 16. (**a**) Coexisting attractors and (**b**) related time series of the incommensurate fractional-order system (17). The parameter values are derived from Table 1. The initial conditions are specified as $(y_1(0), 0.3, 0.4, 0)$ where $y_1(0) \in \{14, 15, 16\}$. The three instances are depicted using green, blue, and red curves.

Without changing the system parameters, the incommensurate fractional-order power system's operating point may fluctuate due to coexistence or multistable behavior. This change raises the possibility that the SSG will either progress toward persistent or chaotic oscillatory behavior or settle into a regular equilibrium.

These findings indicate that the dynamical behavior of the considered incommensurate fractional-order power system is highly dependent not only on the system parameters and fractional orders but also on the initial conditions. The observed coexistence of attractors demonstrates the presence of multiple stable operating regimes under identical parameter settings. From a practical perspective, this sensitivity may affect the predictability and reliability of power system operation, since small variations in the initial state can lead to significantly different long-term responses. Therefore, understanding and controlling such multistable behaviors is essential for ensuring stable system performance.

The sensitivity of the system dynamics to the initial conditions has been partially investigated through the multistability analysis. The obtained coexisting attractors demonstrate that different initial conditions may lead to distinct long-term dynamical behaviors under identical parameter values. These results indicate that the observed dynamics are not exclusively associated with the initial condition $(15, 0.3, 0.4, 0)$ but persist for different initial states, highlighting the sensitivity of the incommensurate fractional-order power system to its initial conditions.

6. Chaos Control

From an engineering perspective, chaotic oscillations in power systems are generally undesirable because they may degrade power quality, reduce system reliability, and threaten secure operation. The presence of chaos implies a high sensitivity to initial conditions and parameter variations, which can lead to unpredictable system responses. Therefore, an effective control strategy is required to suppress chaotic oscillations and drive the system toward a stable operating state. The objective of the proposed controller is not only to demonstrate the controllability of the incommensurate fractional-order power system but also to improve its dynamical stability and ensure reliable operation under chaotic conditions. It should be emphasized that the objective of this section is not to introduce a new control design methodology. Rather, the proposed controller is employed as a proof-of-concept framework to demonstrate that the chaotic dynamics generated by the incommensurate fractional-order power system can be effectively suppressed and steered toward a stable operating condition. Before creating the controlled fractional power model, we describe the primary stability frameworks relevant to incommensurate fractional-order continuous-time systems.

We investigate an n-dimensional nonlinear fractional-order system in the Caputo sense described by

$$\begin{cases} {}^{C}D_t^{q_1} y_1(t) = k_1(y_1, y_2, \ldots, y_n), \\ {}^{C}D_t^{q_2} y_2(t) = k_2(y_1, y_2, \ldots, y_n), \\ \qquad \vdots \\ {}^{C}D_t^{q_n} y_n(t) = k_n(y_1, y_2, \ldots, y_n), \end{cases} \qquad 0 < q_i \leq 1, \;\; i = 1, 2, \ldots, n. \tag{19}$$

Here, ${}^{C}D_t^{q_i}$ denotes the Caputo fractional derivative of order q_i. Let $\tau^\star = (\tau_1^\star, \ldots, \tau_n^\star)$ be an equilibrium point satisfying $h_i(\tau^\star) = 0$ for all $i = 1, \ldots, n$. Assume that each k_i is continuously differentiable in a neighborhood of $\tau^\star$. Define the Jacobian matrix at $\tau^\star$ by

$$G(\tau^\star) = \left[\frac{\partial k_i}{\partial x_j}(\tau^\star)\right]_{i,j=1}^{n}. \tag{20}$$

Theorem 1 ([24])**.** *Consider an n-dimensional fractional-order continuous-time system of* incommensurate *order, i.e., q_i for some $i = 1, 2, 3, 4$. Assume that the fractional orders are rational numbers,*

$$q_i = \frac{\ell_i}{s_i}, \qquad 0 < \ell_i < s_i, \quad \ell_i, s_i \in \mathbb{N}, \quad i = 1, \ldots, n. \tag{21}$$

Let

$$s = \mathrm{lcm}(s_1, s_2, \ldots, s_n), \qquad \delta_i = s\, q_i \in \mathbb{N}. \tag{22}$$

Then, the equilibrium point $y^\star$ is locally asymptotically stable *if all roots λ of the characteristic equation*

$$\det\Big(\mathrm{diag}(\lambda^{\delta_1}, \lambda^{\delta_2}, \ldots, \lambda^{\delta_n}) - G(\tau^\star)\Big) = 0 \tag{23}$$

satisfying

$$|\arg(\lambda)| > \frac{\pi}{2s}. \tag{24}$$

To stabilize the continuous-time fractional power system and drive its states asymptotically toward the origin, suitable control inputs are implemented, particularly for formulations with incommensurate fractional orders.

To focus on the stabilization objective, a nonlinear state-feedback controller is constructed. Such controllers are commonly adopted in nonlinear dynamical systems to investigate the possibility of chaos suppression and equilibrium stabilization.

Let

$$Y(t) = \begin{bmatrix} y_1(t) & y_2(t) & y_3(t) & y_4(t) \end{bmatrix}^T,$$

and denote the control input by

$$U(t) = \begin{bmatrix} \varsigma_1(t) & \varsigma_2(t) & \varsigma_3(t) & \varsigma_4(t) \end{bmatrix}^T.$$

The controlled system can therefore be expressed in the compact form

$$D_t^q Y = F(Y) + U.$$

The proposed controller is a nonlinear state-feedback law of the form

$$U = \Phi(Y),$$

where $\Phi(\cdot)$ is designed to cancel the nonlinear terms and stabilize the equilibrium.

Proposition 1. *Consider the controlled continuous fractional-order system given by a fractional-order nonlinear system.*

$$\begin{cases} D_t^{q_1} y_1 = y_2 + \varsigma_1(t), \\ D_t^{q_2} y_2 = p_2 - (D_2 + K_f) y_2 - \beta_{21} \sin(y_1) - \beta_{23} \sin(y_1 - y_3) + \varsigma_2(t), \\ D_t^{q_3} y_3 = y_4 + \varsigma_3(t), \\ D_t^{q_4} y_4 = p_3 - (D_3 + K_f) y_4 - \beta_{31} \sin(y_3) - \beta_{32} \sin(y_3 - y_1) + \varsigma_4(t), \end{cases} \tag{25}$$

where $0 < q_i < 1$, $i = 1,2,3,4$. *Then, the incommensurate fractional power system is locally asymptotically stable under the nonlinear feedback control laws*

$$\begin{cases} \varsigma_1(t) = -y_1, \\ \varsigma_2(t) = \beta_{21}\sin(y_1) + \beta_{23}\sin(y_1 - y_3) - p_2, \\ \varsigma_3(t) = -y_3, \\ \varsigma_4(t) = \beta_{31}\sin(y_3) + \beta_{32}\sin(y_3 - y_1) - p_3. \end{cases} \tag{26}$$

The proposed feedback law is constructed according to the feedback linearization principle. Specifically, each controller component cancels the corresponding nonlinear and constant terms appearing in the uncontrolled dynamics, while introducing stabilizing linear terms. Consequently, the closed-loop system is transformed into a linear fractional-order system whose stability can be analyzed directly using Theorem 1.

Proof. Substituting (26) into (25), the nonlinear and constant terms are completely canceled, yielding the closed-loop system

$$\begin{cases} D_t^{q_1} y_1 = y_2 - y_1, \\ D_t^{q_2} y_2 = -(D_2 + K_f)y_2, \\ D_t^{q_3} y_3 = y_4 - y_3, \\ D_t^{q_4} y_4 = -(D_3 + K_f)y_4. \end{cases} \tag{27}$$

Let

$$\iota_1 = D_2 + K_f > 0, \qquad \iota_2 = D_3 + K_f > 0.$$

Let $Y(t) = (y_1(t), y_2(t), y_3(t), y_4(t))^\top$. Linearizing system (27) around the equilibrium point

$$\tau^\star = (0,0,0,0)$$

yields the Jacobian matrix

$$G(\tau^\star) = \begin{pmatrix} -1 & 1 & 0 & 0 \\ 0 & -\iota_1 & 0 & 0 \\ 0 & 0 & -1 & 1 \\ 0 & 0 & 0 & -\iota_2 \end{pmatrix}. \tag{28}$$

Assume that the fractional orders are rational numbers of the form.

$$q_i = \frac{\ell_i}{s_i}, \qquad 0 < \ell_i < s_i, \qquad i = 1,2,3,4.$$

Let

$$s = \operatorname{lcm}(s_1, s_2, s_3, s_4), \qquad \delta_i = s q_i \in \mathbb{N}.$$

Substituting the Jacobian matrix (28) into the characteristic equation given in Theorem 1 yields

$$\det\Big(\operatorname{diag}(\lambda^{sq_1}, \lambda^{sq_2}, \lambda^{sq_3}, \lambda^{sq_4}) - G(\tau^\star)\Big) = 0. \tag{29}$$

First, we take $q_1 = 0.95$, $q_2 = 1$, $q_3 = 1$, $q_4 = 1$ and $(D_2, D_3, K_f) = (0.2, 0.5, 0.008)$. Then we have $s = 20$

$$\det\Big(\operatorname{diag}(\lambda^{19}, \lambda^{20}, \lambda^{20}, \lambda^{20}) - G(\tau^\star)\Big) = 0. \tag{30}$$

Since the Jacobian matrix has a block upper-triangular structure, its determinant can be factorized into the product of the diagonal block determinants, leading to

$$(\lambda^{19}+1)(\lambda^{20}+\iota_1)(\lambda^{20}+1)(\lambda^{20}+\iota_2)=0. \tag{31}$$

All eigenvalues satisfy the condition.

$$|\arg(\lambda_i)| > \frac{\pi}{40}.$$

Therefore, the fractional continuous-time power system satisfies the stability condition under the proposed criterion. These results demonstrate that the proposed control scheme successfully suppresses chaotic oscillations and stabilizes the system equilibrium, highlighting its potential usefulness for maintaining stable operation of fractional-order power systems. □

Figure 17 illustrates the effectiveness of the proposed controller. Starting from initial conditions corresponding to a chaotic regime, all state trajectories converge asymptotically toward the equilibrium point, confirming the successful suppression of chaotic oscillations and restoration of stable system behavior.

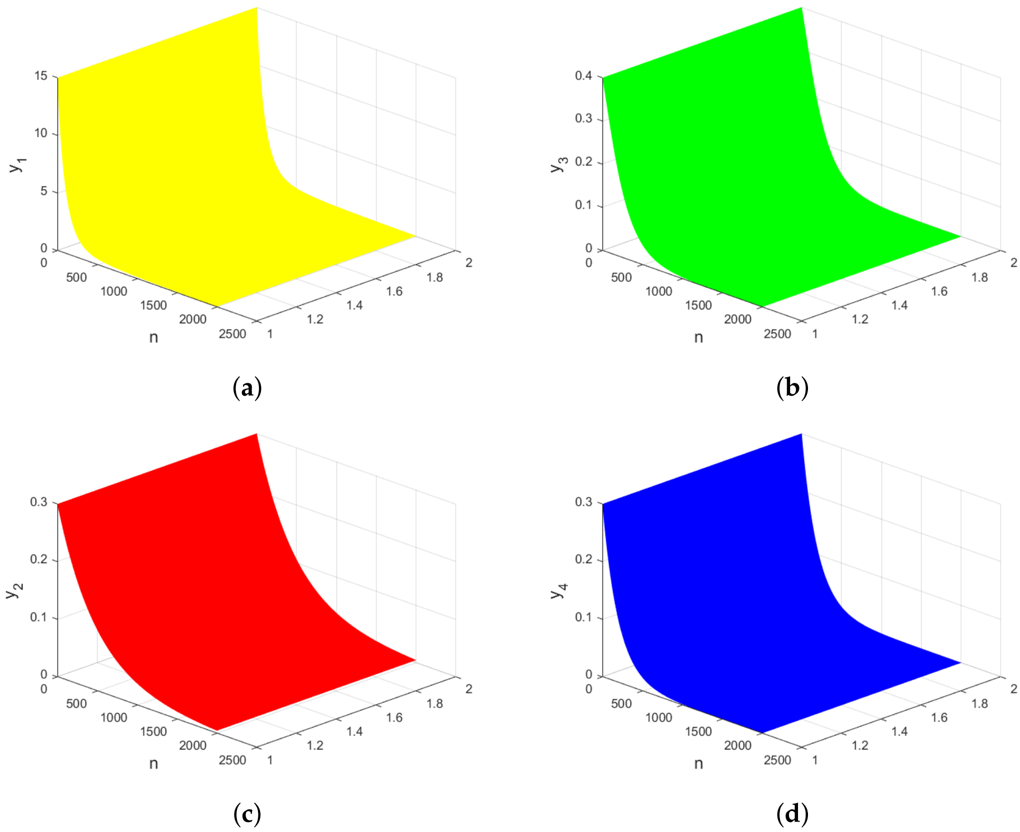

Figure 17. The Stabilized state trajectories of the controlled system for $q_1 = 0.95$, $q_2 = q_3 = q_4 = 1$, with initial conditions $(15, 0.3, 0.4, 0.3)$, $D_2 = 0.2$, $D_3 = 0.5$, and $K_f = 0.008$: (**a**) y_1, (**b**) y_2, (**c**) y_3, and (**d**) y_4.

Several control strategies have been proposed for suppressing chaos in fractional-order systems, including state-feedback control, PI controllers, adaptive control, and observer-based approaches. Compared with these methods, the proposed nonlinear state-feedback controller possesses two main advantages. First, the nonlinear terms are explicitly canceled, resulting in a simple closed-loop system whose stability can be rigorously verified using the incommensurate fractional-order stability theorem. Second, the controller requires only direct measurements of the system states and avoids the additional observer dynamics or parameter adaptation required by more sophisticated methods. Therefore, although the controller is intended primarily as a proof-of-concept, it provides an effective and computationally simple approach for stabilizing the considered fractional-order power system.

7. Conclusions and Perspectives

In this study, a power system model based on the traditional N-machine power system framework is presented, and an incommensurate fractional-order analysis is performed using the Caputo technique. The findings show a range of intricate dynamical behaviors that appear under particular parameter settings and incommensurate fractional-order values, such as period-one oscillations, period-doubling events, chaotic dynamics, and angle instability. Qualitative and quantitative analytical techniques are utilized to characterize these behaviors. In addition, the existence of coexisting attractors and multistability is confirmed through bifurcation diagrams, phase portraits, and time-series analyses. The findings clearly indicate that chaos and multistability are intrinsic features of the incommensurate fractional-order power system. Such phenomena are of significant concern due to their potential to induce unpredictable and uncontrollable system responses, leading to power outages, equipment deterioration, and safety risks. Consequently, effective strategies for monitoring, managing, and controlling chaotic and multistable dynamics are essential to ensure the safe and reliable operation of practical power systems.

Author Contributions: Conceptualization, N.D.; Methodology, O.K. and M.A.; Software, M.A.; Validation, A.O.; Formal Analysis, S.A.; Investigation, S.A.; Writing—Original Draft, O.K. and N.D.; Writing—Review and Editing, A.O. and L.E.A.; Visualization, L.E.A. All authors have read and agreed to the published version of the manuscript.

Funding: Princess Nourah bint Abdulrahman University Researchers Supporting Project number (PNURSP2026R831), Princess Nourah bint Abdulrahman University, Riyadh, Saudi Arabia. The authors extend their appreciation to the Deanship of Scientific Research at Northern Border University, Arar, KSA for funding this research work through the project number "NBU-FPEJ-2026-2443-06".

Data Availability Statement: The original contributions presented in this study are included in the article. Further inquiries can be directed to the corresponding authors.

Acknowledgments: Princess Nourah bint Abdulrahman University Researchers Supporting Project number (PNURSP2026R831), Princess Nourah bint Abdulrahman University, Riyadh, Saudi Arabia. The authors extend their appreciation to the Deanship of Scientific Research at Northern Border University, Arar, KSA for funding this research work through the project number "NBU-FPEJ-2026-2443-06".

Conflicts of Interest: The authors declare no conflict of interest.

References

1. Ma, H.; Min, F.; Wang, Y. Nonlinear dynamic analysis and surface sliding mode controller based on low-pass filter for chaotic oscillation in a power system with power disturbance. *Chin. J. Phys.* **2018**, *56*, 2488–2499. [CrossRef]
2. Samuel, I.A.; Katende, J.; Awosope, C.O.A.; Awelewa, A.A. Prediction of voltage collapse in electrical power system networks using a new voltage stability index. *Int. J. Appl. Eng. Res.* **2017**, *12*, 190–199.
3. Yu, Y.; Jia, H.; Li, P.; Su, J. Power system instability and chaos. *Electr. Power Syst. Res.* **2003**, *65*, 187–195. [CrossRef]
4. Gholizadeh, H.; Hassannia, A.; Azarfar, A. Chaos detection and control in a typical power system. *Chin. Phys. B* **2013**, *22*, 010503. [CrossRef]
5. Vahdati, P.M.; Kazemi, A. Bifurcations and chaos in nonlinear dynamics of power systems. In Proceedings of the 24th Iranian Conference on Electrical Engineering (ICEE), Shiraz, Iran, 10–12 May 2016; pp. 1706–1711.
6. Wang, X.; Lu, Z.; Song, C. Chaotic threshold for a class of power system model. *Shock Vib.* **2019**, *2019*, 3479239. [CrossRef]

7. Almeida, A.M.d.; Lenzi, M.K.; Lenzi, E.K. A Survey of fractional order calculus applications of multiple-input, multiple-output (MIMO) process control. *Fractal Fract.* **2020**, *4*, 22. [CrossRef]
8. Sharafian, A.; Ullah, I.; Singh, S.K.; Ali, A.; Khan, H.; Bai, X. Adaptive fuzzy backstepping secure control for incommensurate fractional-order cyber-physical power systems under intermittent denial of service attacks. *Chaos Solitons Fractals* **2024**, *186*, 115288. [CrossRef]
9. Wang, P.; Chen, X.; Zhang, Y.; Zhang, L.; Huang, Y. Fractional-Order Load Frequency Control of an Interconnected Power System with Hydrogen Energy-Storage Unit. *Preprints* **2024**. [CrossRef]
10. Fathollahi, A.; Andresen, B. Enhancing Transient Stability in Multi-Machine Power Systems through a Model-Free Fractional-Order Excitation Stabilizer. *Fractal Fract.* **2024**, *8*, 419. [CrossRef]
11. Kahouli, O.; Zouak, I.; Almohaimeed, S.; Ouannas, A.; Amraoui, L.E.; Ayari, M. On Fractional Discrete-Time Power Systems: Chaos, Complexity and Control. *Mathematics* **2026**, *14*, 1354. [CrossRef]
12. Chen, Y. Applied fractional calculus in controls. In *2009 American Control Conference*; IEEE: Piscataway, NJ, USA, 2009; pp. 34–35.
13. Chang, S.-C. Stability, Chaos Detection, and Quenching Chaos in the Swing Equation System. *Math. Probl. Eng.* **2020**, *2020*, 6677084. [CrossRef]
14. Chang, S.-C. Controlling Chaos through Period-Doubling Bifurcations in Attitude Dynamics for Power Systems. *Math. Probl. Eng.* **2020**, *2020*, 8853459. [CrossRef]
15. Gupta, P.C.; Singh, P.P. Multistability, multiscroll chaotic attractors and angle instability in multi-machine swing dynamics. *IFAC PapersOnLine* **2022**, *55*, 572–578. [CrossRef]
16. Gupta, P.C.; Singh, P.P. Multistability, coexisting behaviours and control of fractional order dissipative small scale grid with disturbances and noise. *Eur. Phys. J. Spec. Top.* **2023**, *232*, 2415–2436. [CrossRef]
17. Gupta, P.C.; Singh, P.P. Chaos and Multistability in Fractional Order Power System: Dynamic Analysis and Implications. In *Innovations in Electrical and Electronic Engineering*; Lecture Notes in Electrical Engineering; Springer: Berlin/Heidelberg, Germany, 2024; Volume 1109.
18. Podlubny, I. *Fractional Differential Equations*; Academic Press: New York, NY, USA, 1999.
19. Tavazoei, M.S.; Haeri, M. Chaotic attractors in incommensurate fractional order systems. *Phys. D Nonlinear Phenom.* **2008**, *237*, 2628–2637. [CrossRef]
20. Deng, W.; Li, C.; Lu, J. Stability analysis of linear fractional differential system with multiple time delays. *Nonlinear Dyn.* **2007**, *48*, 409–416. [CrossRef]
21. Kopell, N.; Washburn, R. Chaotic motions in the two-degree- of-freedom swing equations. *IEEE Trans. Circuits Syst.* **1982**, *29*, 738–746.
22. Chang, S.C. Study of Structural Stability for Power System. Master's Thesis, National Central University, Taoyuan City, Taiwan, 1992.
23. Baleanu, D.; Diethelm, K.; Scalas, E.; Trujillo, J. *Fractional Calculus Models and Numerical Methods*; World Scientific Publishing Company: Singapore, 2012.
24. Odibat, Z.; Corson, N.; Aziz-Alaoui, M.A.; Alsaedi, A. Chaos in Fractional Order Cubic Chua System and Synchronization. *Int. J. Bifurc. Chaos* **2017**, *27*, 1750161. [CrossRef]